Nuclear Engineering and Technology 55 (2023) 3206–3212

Contents lists available at ScienceDirect

Nuclear Engineering and Technology

journal homepage: www.elsevier.com/locate/net

Original Article

Feasibility study on fiber-optic inorganic scintillator array sensor system for multi-dimensional scanning of radioactive waste

Jae Hyung Park [a], Siwon Song [a], Seunghyeon Kim [a], Jinhong Kim [a], Seunghyun Cho [b], Cheol Ho Pyeon [c], Bongsoo Lee [a, *]

[a] School of Energy Systems Engineering, Chung-Ang University, Seoul, 06974, South Korea
[b] Department of Organic Materials and Fiber Engineering, College of Engineering, Soongsil University, Seoul, 156-743, South Korea
[c] Research Center for Safe Nuclear System, Institute for Integrated Radiation and Nuclear Science, Kyoto University, Asashiro-nishi, Kumatori-cho, Sennan-gun, Osaka, 590-0494, Japan

ARTICLE INFO

Article history:
Received 18 April 2023
Received in revised form
25 May 2023
Accepted 1 June 2023
Available online 1 June 2023

Keywords:
Radioactive waste
Scanning method
Inorganic scintillator array
Plastic optical fiber
Multi-dimensional
Remote sensing

ABSTRACT

We developed a miniaturized multi-dimensional radiation sensor system consisting of an inorganic scintillator array and plastic optical fibers. This system can be applied to remotely obtain the radioactivity distribution and identify the radionuclides in radioactive waste by utilizing a scanning method. Variation in scintillation light was measured in two-dimensional regions of interest and then converted into radioactivity distribution images. Outliers present in the images were removed by using a digital filter to make the hot spot location more accurate and cubic interpolation was applied to make the images smoother and clearer. Next, gamma-ray spectroscopy was performed to identify the radionuclides, and three-dimensional volume scanning was also performed to effectively find the hot spot using the proposed array sensor.

1. Introduction

With the utilization of radiation and nuclear materials in various fields, such as medicine, industry, and nuclear facilities, it is expected that radioactive waste generation will increase [1]. In addition, as nuclear power plants are being actively decommissioned worldwide, the importance of radioactive waste management is increasing [2]. Radioactive waste must be managed through several stages, from generation to final disposal, and the characteristics of the waste need to be classified and verified to meet the acceptance criteria at each stage [3,4]. To verify the nuclide inventory of radioactive waste, non-destructive assay techniques such as segmented gamma scanning are routinely used [5].

A high-purity germanium detector (HPGe) is typically used in non-destructive assays due to its excellent energy resolution that enables accurate acquisition of radionuclide information via gamma-ray spectroscopy [6]. However, its use is restricted in many fields due to the various incidental disadvantages of using cryogenic cooling to prevent thermal excitation [7]. The mobility of an HPGe detector is limited due to its large volume and weight including cryostat, and the detector package geometry is standardized for cooling, which makes it difficult to use it in many target environments and conditions. In addition, it has other disadvantages of a slow response due to the required cool-down time of several hours and high price. Thus, there is a need to develop a detection system for radioactive waste that is easier to manage, has a short response time, is cost-effective, and is adaptable for use in various target environments and conditions.

Inorganic scintillators are widely used in various fields that require high geometric efficiency and sensor miniaturization due to their high density, light yield, and machinability in diverse forms [8]. Although hygroscopicity is the biggest disadvantage of inorganic scintillators, cerium-doped scintillators such as GAGG:Ce and LYSO:Ce have shown good performance without this drawback [9–12].

Several studies have been conducted on developing fiber-optic radiation sensors with small inorganic scintillators. Han et al. fabricated a fiber-optic radiation sensor (FORS) with a plastic optical fiber (POF) and three different inorganic scintillators (BGO,

* Corresponding author.
E-mail address: bslee@cau.ac.kr (B. Lee).

https://doi.org/10.1016/j.net.2023.06.002

YSO:Ce, and LYSO:Ce), to measure radiation levels on-site [13]. Yoo et al. evaluated the ability of a FORS to distinguish radionuclides in a mixed radiation field [14], while Song et al. demonstrated the effect of the length of the optical fiber on changes in the gamma-ray energy spectrum of Cs-137 and the energy resolution of a FORS [15]. In the medical field, fiber-optic dosimetry (FOD) or optical fiber sensor (OFS) have been utilized for real-time *in vivo* measurements during radiotherapy, for which they have shown good response stability, a linear energy response, and high spatial resolution [16–18]. Building upon these advantages, researchers have also conducted studies to develop fiber-optic sensors or fiber-shaped scintillators in the form of bundles or arrays for radiation-imaging purposes [19–21].

POFs offer several advantages when being used for radiation sensing, such as having a small sensing part, being lightweight, and being of sufficiently long length with good flexibility, which makes them suitable for use in narrow, complex, and curved conditions. They can also be used to monitor a large area with many point detections and are resistant to moisture, corrosion, and electromagnetic interference, making them usable in harsh environments [22,23]. In addition, many recently developed sensing materials can be made into fiber shapes, which makes it easy to fabricate combined sensors, as well as improving accuracy and lowering the fabrication cost [24,25].

In this study, we developed an inorganic scintillator array sensor system with a POF for acquiring radioactivity distribution and hot spot location in radioactive waste by utilizing a scanning method. For sensor miniaturization and combining with POF for remote sensing, we used a non-hygroscopic inorganic scintillator, GAGG:Ce, to fabricate an array-form sensor. Variation in scintillation lights was measured in two-dimensional regions of interest (ROIs) and then converted into a radioactivity distribution image. Outliers present in the image were removed by using a digital filter to obtain the hot spot location more accurately and cubic interpolation was applied to make the images smoother and clearer. Meanwhile, gamma-ray spectroscopy was performed to identify radionuclides, and three-dimensional volume scanning was also performed that could effectively find hot spots using the proposed array sensor.

2. Materials and methods

We used a GAGG:Ce scintillator (GAGG-HL, Epic Crystal) as the sensing element for direct coupling with a POF. Because of its non-hygroscopicity, GAGG:Ce can be utilized without housing and is suitable for small-volume applications. In addition, it has many advantages for use in gamma-ray sensing, such as high density and effective Z-number, and high light yield and sensitivity. The physical properties of GAGG:Ce are listed in Table 1 [26].

Table 1
The physical properties of GAGG:Ce.

Property	Value
Density (g/cm^3)	6.63
Effective Z-number	54
Decay time (ns)	150
Light yield (photons/MeV)	~54,000
Emission wavelength peak (nm)	530
Hygroscopicity	None

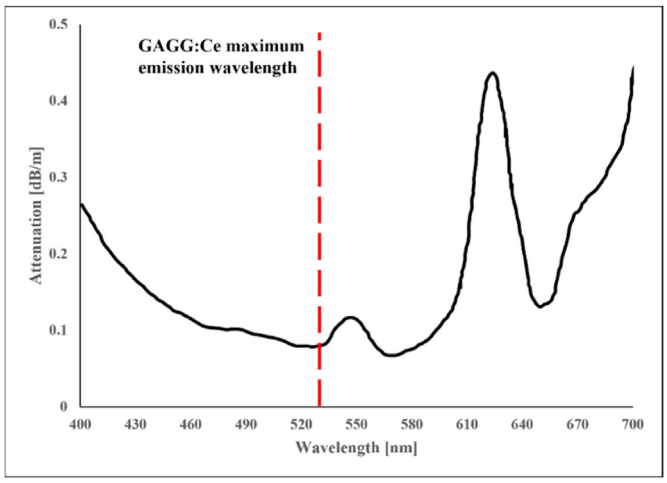

Fig. 1. The attenuation rate of the plastic optical fiber.

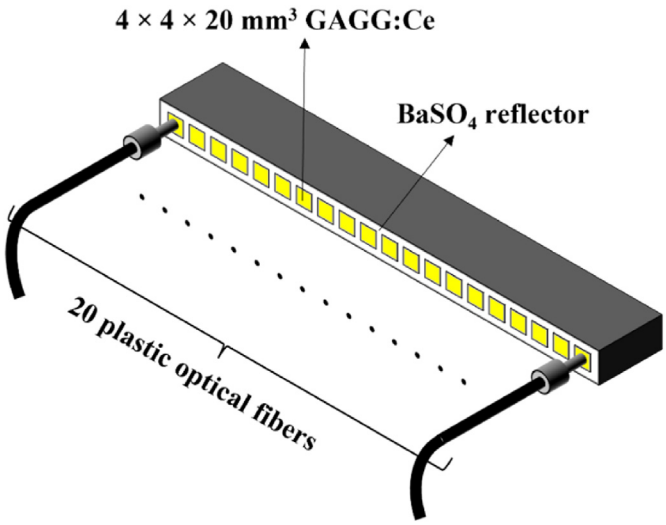

Fig. 2. A schematic diagram of the GAGG:Ce array sensor.

Another advantage of GAGG:Ce can be observed at its maximum emission wavelength. Fig. 1 shows the attenuation rate of the POF used in this study (CK-120, Mitsubishi Chemical) according to the wavelength of the light signal [27]. It is confirmed that the rate of attenuation is very low at 530 nm, the maximum emission wavelength of GAGG:Ce. This means that the scintillation light from GAGG:Ce can be transmitted through the POF with low loss.

A schematic diagram of the GAGG:Ce array sensor is depicted in Fig. 2. For this study, 20 GAGG:Ce crystals with dimensions of $4 \times 4 \times 20$ mm^3 were arranged in parallel. To optimize scintillation light collection and prevent optical crosstalk between the scintillators, each scintillator in the array was covered with a 1 mm thick $BaSO_4$ reflector. The centers of the crystals were 5 mm apart, resulting in a total array size of $101 \times 6 \times 21$ mm^3. Each crystal was connected to the photodetector through a 1 m long POF, and optical pads (EJ-560, Eljen Technology) were applied at the scintillator-POF and POF-photodetector interfaces to ensure optimal light transmission through refractive index matching and tight contact.

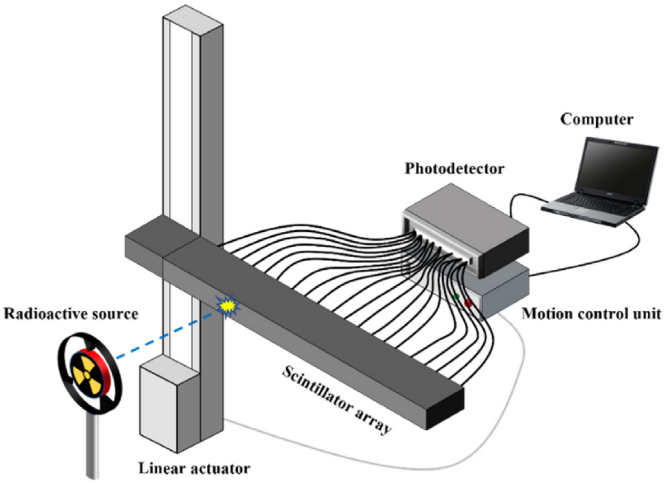

Fig. 3. The experimental setup for two-dimensional vertical scanning.

The experimental setup for two-dimensional vertical scanning is presented in Fig. 3. The array sensor was connected to a linear actuator (LEFS25RA-300, SMC) to construct a system capable of vertical scanning. The light generated from the scintillator was transmitted through the POF to the photodetector, where it was expressed as a quantitative count by the photon counting circuit. A photon counting head (H11890-210, Hamamatsu) equipped with a high-speed photon counting circuit and high count sensitivity at the 530 nm wavelength of GAGG:Ce was used as the photodetector [28]. The vertical scanning interval was set to 5 mm, which corresponds to the interval between the centers of the scintillators in the array.

3. Experimental results

Fig. 4 presents the results of two-dimensional vertical scanning, showing the scintillation light output variation based on the sensor height. In this experiment, we used a 43.21 μCi Co-60 gamma-ray source and the legend in Fig. 4(a) indicates that 0 mm represents when the gamma-ray source and the sensor are on the same horizontal line. In Fig. 4(a), count differences can be clearly observed

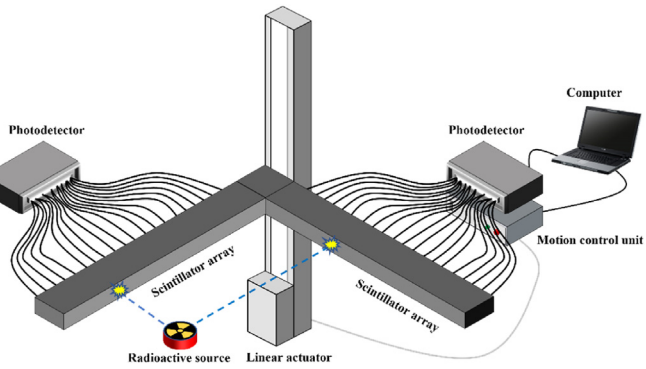

Fig. 5. The experimental setup for two-dimensional horizontal measurements.

with respect to the sensor height and the distance between the centers of the scintillators. Fig. 4(b) visualizes of Fig. 4(a) on an RGB scale, where each pixel represents the count at the position, and the redder color indicates a higher count. Since the scintillation count is proportional to the amount of radiation interacting with the scintillator, Fig. 4(b) presents the radioactivity distribution of the measurement area. The reddest spot in Fig. 4(b) denotes the hot spot where the level of radiation is higher than the surrounding area, and it was observed to be located at channel number 10 with a height of 0 mm.

Two-dimensional horizontal scanning was subsequently carried out, and the experimental setup for horizontal measurements is presented in Fig. 5. Two GAGG:Ce array sensors were combined in an L-shape, and the scintillation light was measured after a gamma-ray source was positioned within its 101 × 101 mm^2 measurement area. During the measurements, the radioactive source and the sensor were positioned on the same horizontal line and their height was fixed.

Fig. 6 shows changes in radioactivity distribution in the two-dimensional horizontal plane according to the position of the source. The small circle in the figure represents the actual location of the radiation source, and the diameter of the active element inside the source disc is 5 mm. The measured counts from the sensors forming the horizontal and vertical axes of the measurement area were combined, and it can be observed that the hot spot

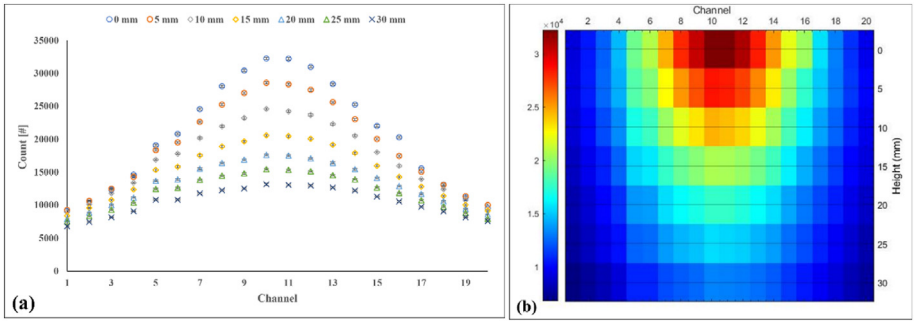

Fig. 4. The results of two-dimensional vertical scanning with the proposed sensor. (a) Scintillation light output variations by vertical scanning of the sensor array at different heights. (b) Visualization of the results in (a) using an RGB scale.

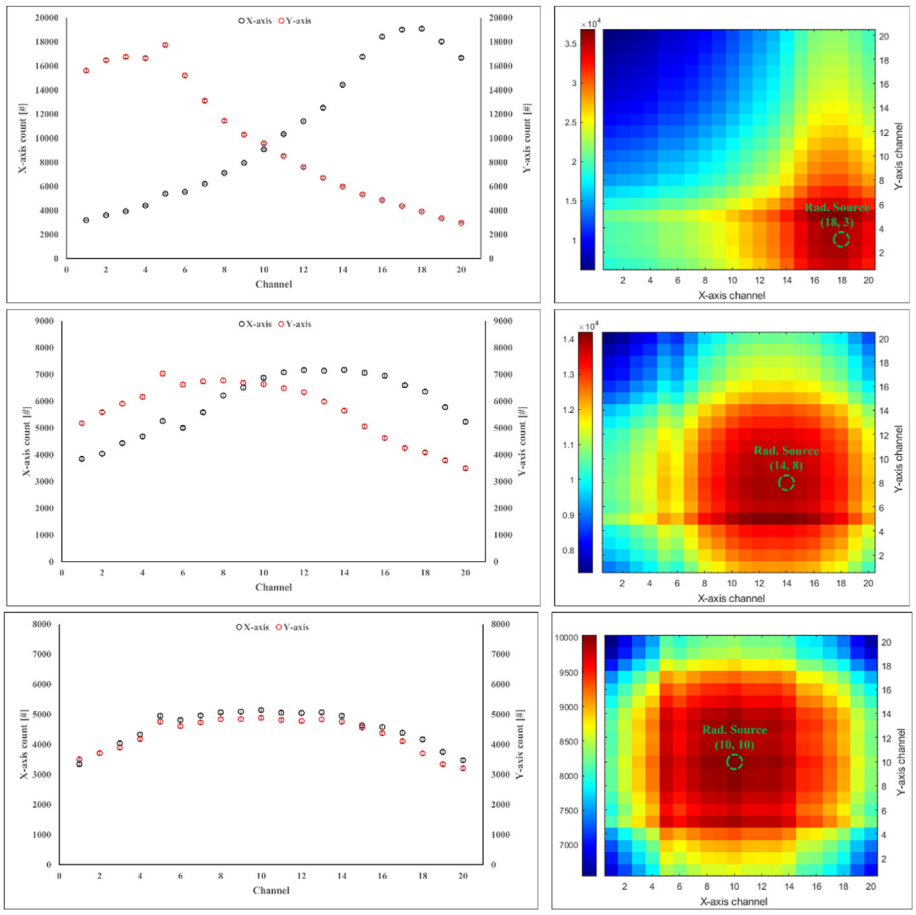

Fig. 6. Changes in two-dimensional radioactivity distribution according to the position of the radioactive source.

moves according to changes in the position of the gamma-ray source, causing changes in the radioactivity distribution in the area. Although the location of the hot spot can be easily identified in Fig. 6, the reddest point was not in the expected position due to outliers, which are abnormal values in certain spots that masked the exact location of the radioactive source. Therefore, removing these outliers was necessary.

Fig. 7 shows the outcomes of applying a Savitzky-Golay (SG) filter and cubic interpolation sequentially to the radioactivity distribution images. The SG filter is a commonly used digital filter for signal smoothing that is effective at reducing noise, including outliers, through convolution and is also widely utilized in image processing [29,30]. In comparison with the original images, it can be observed that the SG filter removed the outliers and corrected the position of the hot spot while cubic interpolation made the images smoother and clearer.

To identify nuclides in a radioactive source, it is necessary to acquire an energy spectrum by using gamma-ray spectroscopy. For clear energy spectrum measurements, gamma-rays and the detector must interact sufficiently, and the simplest way to achieve this is to bring the detector as close to the radioactive source as possible.

After image enhancement, gamma-ray spectroscopy was performed using the channel closest to the hot spot. This was achieved using a photomultiplier tube (PMT; R6233-100, Hamamatsu) with high sensitivity at 530 nm and a low dark current of 2 nA. The current signal generated by the PMT was converted into an amplified voltage signal via a charge-sensitive preamplifier (Model 2005, Mirion). This signal was then sorted and rearranged into a spectrum based on its amplitude using a digitizer (DT5725, Caen) employing a trapezoidal filter.

Fig. 8 shows the acquired energy spectra using the closest sensor channel to the hot spot for Cs-137 and Co-60 gamma-ray sources having activities of 40.53 and 43.21 μCi, respectively. The full energy peaks of the radionuclides were measured: the energy resolutions were estimated as 10.34%, 7.24%, and 7.18% at 662, 1,173, and 1,332 keV, respectively. The relationship between the analog-to-digital converter (ADC) channel number and the full energy peak energies of the radionuclides is displayed in Fig. 9, which exhibits good linearity with an R^2 value of around 0.9984. This indicates that the signal generation and amplitude analysis with respect to gamma-ray energies were performed linearly and accurately.

Following the two-dimensional measurements, three-

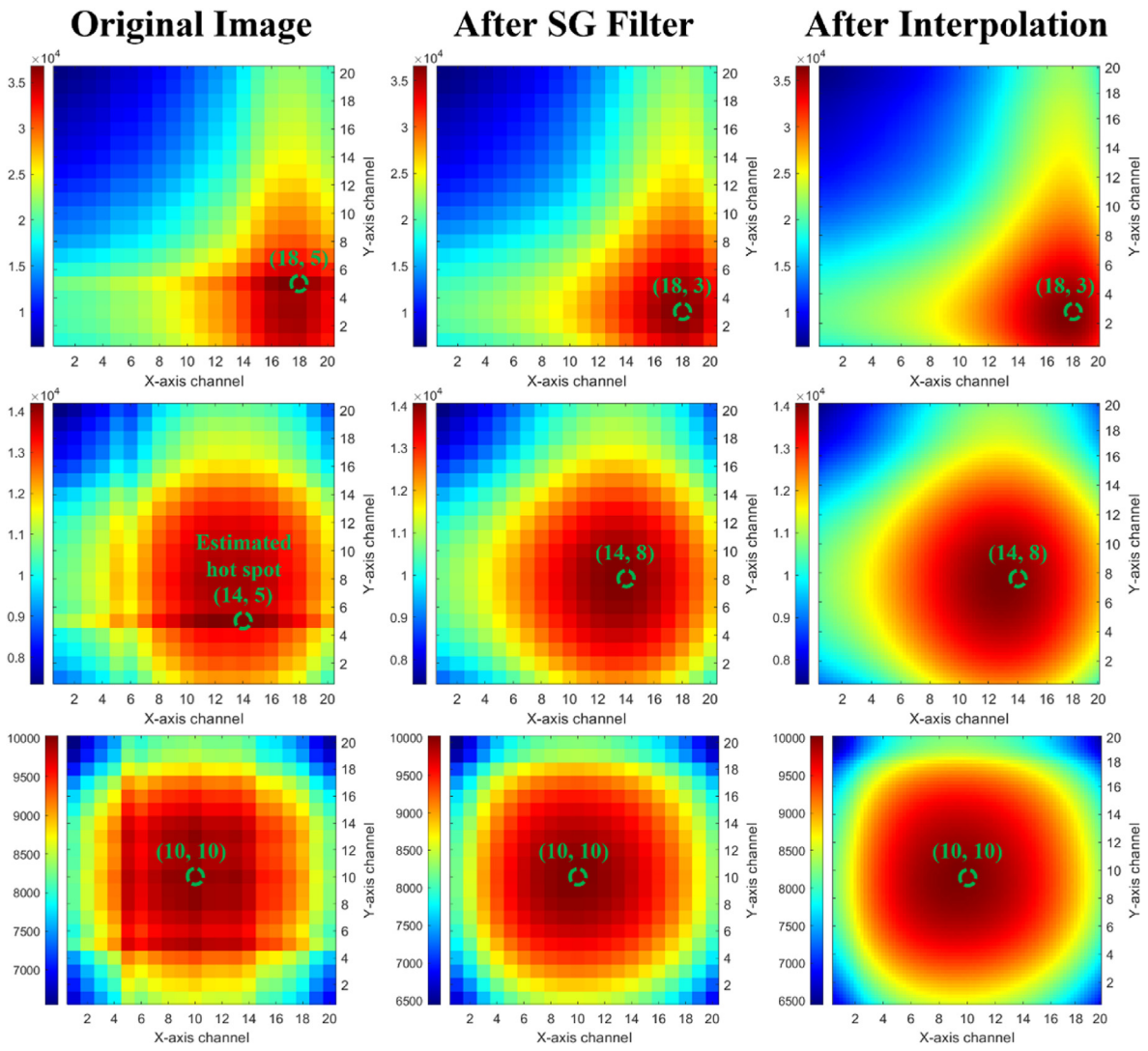

Fig. 7. Application of a Savitzky-Golay filter and cubic interpolation to remove outliers and enhance the images.

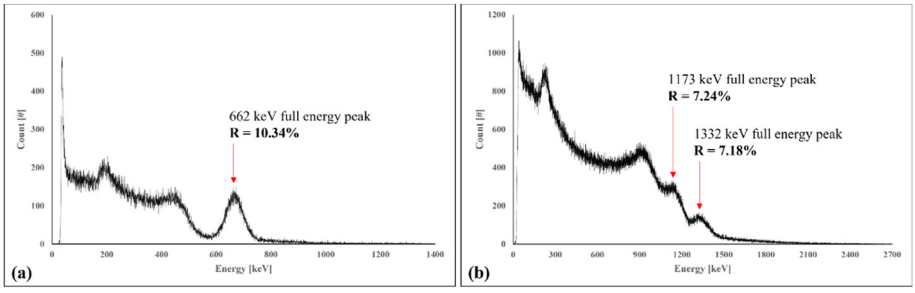

Fig. 8. Acquired energy spectra using the closest channel to the hot spot of (a) Cs-137 and (b) Co-60 radioactive sources.

dimensional scanning was performed using the same configuration as shown in Fig. 5. For three-dimensional measurement, two vertical scans are needed using the L-shaped sensor array. The first scan moves the L-shaped sensor array upward from the lowest to the highest point in 5 mm increments, while the second scan rotates the sensor array by 180° and moves it downward from the highest to the lowest point, again in 5 mm steps. Scintillation light was acquired in four directions and the resulting data were visualized as a distribution image.

Fig. 10 shows the acquired three-dimensional images of the

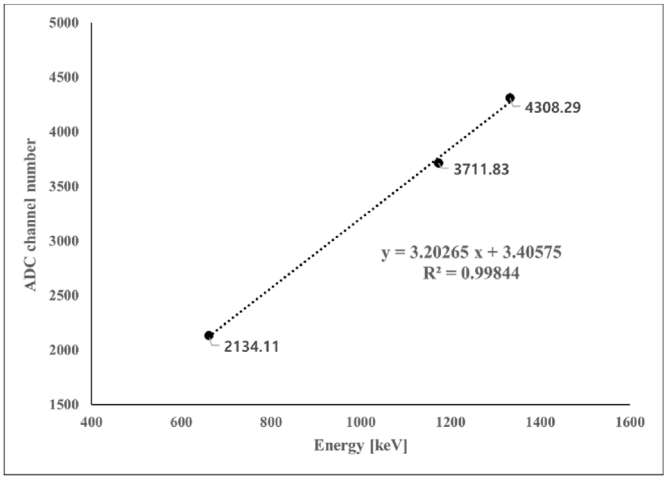

Fig. 9. The relationship between the analog-to-digital converter (ADC) channel number and the full energy peak energies of the radionuclides.

radioactivity distribution and the hot spot. Similar to the two-dimensional image, red indicates a higher radiation level. Thus, the three-dimensional radioactivity distribution within the rectangular parallelepiped ROI can be observed, and the three-dimensional location information of the hot spot was obtained by identifying the points with high counts that represent the top 10% of measured scintillation lights in the entire data.

4. Conclusions

In this study, we developed a miniaturized multi-dimensional radiation sensor system consisting of an inorganic scintillator array and POFs. This system can be applied to remotely obtain the radioactivity distribution and radionuclide information in radioactive waste by utilizing a scanning method. The scintillator array sensor was fabricated using GAGG:Ce, which is characterized by non-hygroscopicity and high light yield.

Variation in scintillation light due to changes in the sensor height and the position of the gamma-ray source was measured and converted into a radioactivity distribution image. The accuracy of hot spot location was improved by applying an SG filter to remove outliers while utilizing cubic interpolation made the images smoother and clearer. Based on the location information, gamma-ray spectroscopy was performed at the nearest sensor channel to the hot spot, and energy spectra of Cs-137 and Co-60 were obtained. The three-dimensional distribution showing the position of the hot spot was also acquired.

Because of the disadvantages of existing detectors used to identify the characteristics of radioactive waste, we conducted a feasibility study to develop a system capable of obtaining the radioactivity distribution and radionuclide information within an ROI. Our proposed system utilizes an inorganic scintillator, which has high radiation detection efficiency and machinability. Although the system may experience some energy resolution loss, it does not require cooling and has excellent degrees of freedom in configuration and handling. Given that the system could obtain point data from the scanning area and identify Cs-137 and Co-60, which are the key nuclides for the scaling factor method, it can potentially be used to supplement existing detectors.

However, the radioactivity distribution images are still blurry and the hot spot appears as much larger than the actual source size. This is because the scintillators are too close together to generate a significant difference in counts with respect to an adjacent uncollimated radioactive source. In future studies, we will investigate the use of collimators on the scintillator array to adjust the count differences between the channels by collimating the incoming gamma-rays. Furthermore, image enhancement techniques will also be studied to improve the quality of the three-dimensional images.

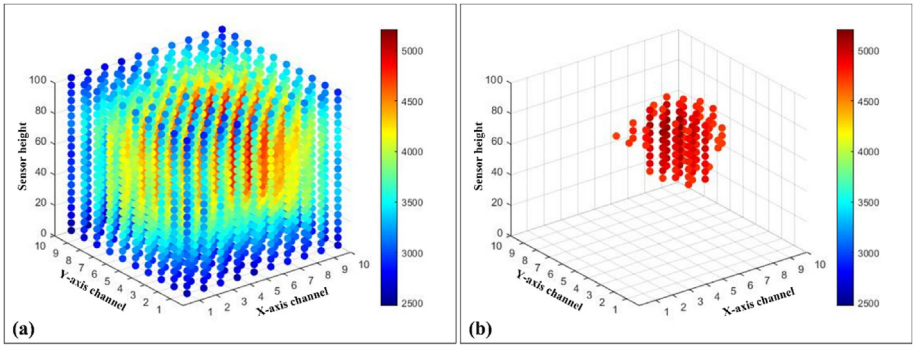

Fig. 10. Acquired three-dimensional images of (a) radioactivity distribution and (b) the hot spot.

Declaration of competing interest

The authors declare no conflict of interest.

Acknowledgements

This research was supported by the Korea Institute of Energy Technology Evaluation and Planning (KETEP) grant funded by the Korean government (MOTIE) (No. 20201520300060) and the National Research Foundation of Korea (NRF) grant funded by the Korean government (MSIT) (No. 2020M2D2A2062457, 2022M2D4A1084440).

References

[1] The International Atomic Energy Agency (IAEA), Status and Trends in Spent Fuel and Radioactive Waste Management, 2018. IAEA Nuclear Energy Series No. NW-T-1.14.
[2] IAEA, Nuclear Technology Review 2022, 2022. IAEA/NTR/2022.
[3] IAEA, Predisposal management of radioactive waste, IAEA Safety Standards Series No, GSR Part 5, IAEA, Vienna, 2009.
[4] IAEA, Classification of Radioactive Waste, IAEA Safety Standards Series No. GSG-1, IAEA, Vienna, 2009, 2009.
[5] IAEA, Strategy and Methodology for Radioactive Waste Characterization, IAEA, Vienna, 2007. IAEA-TECDOC-1537.
[6] D. Reilly, N. Ensslin, H. Smith, Passive Nondestructive Assay of Nuclear Materials, US Nuclear Regulatory Commission, Washington DC, 1991. NUREG/CR-5550.
[7] B.D. Milbrath, A.J. Peurrung, M. Bliss, W.J. Weber, Radiation detector materials: an overview, J. Mater. Res. 23 (2008) 2561–2581, https://doi.org/10.1557/JMR.2008.0319.
[8] P. Lecoq, A. Annenkov, A. Gektin, M. Korzhik, C. Pedrini, Inorganic Scintillators for Detector Systems in Physical Principles and Crystal Engineering, first ed., Springer, Berlin, 2006.
[9] K. Kamada, T. Yanagida, T. Endo, K. Tsutumi, Y. Usuki, M. Nikl, Y. Fujimoto, A. Fukabori, A. Yoshikawa, 2 inch diameter single crystal growth and scintillation properties of Ce:$Gd_3Al_2Ga_3O_{12}$, J. Cryst. Growth 352 (2012) 88–90, https://doi.org/10.1016/j.jcrysgro.2011.11.085.
[10] J. Iwanowska, L. Swiderski, T. Szczesniak, P. Sibczynski, M. Moszynski, M. Grodzicka, K. Kamada, K. Tsutsumi, Y. Usuki, T. Yanagida, A. Yoshikawa, Performance of cerium-doped $Gd_3Al_2Ga_3O_{12}$ (GAGG:Ce) scintillator in gamma-ray spectrometry, Nucl. Instrum. Methods Phys. Res. A 712 (2013) 34–40, https://doi.org/10.1016/j.nima.2013.01.064.
[11] I. Valais, S. David, C. Michail, D. Nikolopoulos, P. Liaparinos, D. Cavouras, I. Kandarakis, G.S. Panayiotakis, Comparative study of luminescence properties of LuYAP:Ce and LYSO:Ce single-crystal scintillators for use in medical imaging, Nucl. Instrum. Methods Phys. Res. A 580 (2007) 614–616, https://doi.org/10.1016/j.nima.2007.05.023.
[12] W. Chewpraditkul, L. Swiderski, M. Moszynski, T. Szczesniak, A. Syntfeld-Kazuch, C. Wanarak, P. Limsuwan, Scintillation properties of LuAG:Ce, YAG:Ce, and LYSO:Ce crystals for gamma-ray detection, IEEE Trans. Nucl. Sci. 56 (2009) 3800–3805, https://doi.org/10.1109/TNS.2009.2033994.
[13] K.-T. Han, W.J. Yoo, J.K. Seo, S.H. Shin, D. Jeon, S. Hong, S. Cho, J.H. Moon, B. Lee, Optical fiber-based gamma-ray spectroscopy with cerium-doped lutetium yttrium orthosilicate crystal, Opt. Rev. 20 (2013) 205–208, https://doi.org/10.1007/s10043-013-0036-z.
[14] W.J. Yoo, S.H. Shin, D.E. Lee, K.W. Jang, S. Cho, B. Lee, Development of a small-sized, flexible, and insertable fiber-optic radiation sensor for gamma-ray spectroscopy, Sensors 15 (2015) 21265–21279, https://doi.org/10.3390/s150921265.
[15] Y.B. Song, S.H. Shin, S.W. Song, H.J. Kim, S. Cho, B. Lee, Feasibility study on remote gamma spectroscopy system with fiber-optic radiation sensor, J. Radioanal. Nucl. Chem. 316 (2018) 1301–1306, https://doi.org/10.1007/s10967-018-5754-z.
[16] N. Martínez, A. Rucci, J. Marcazzó, P. Molina, M. Santiago, W. Cravero, Characterization of $YVO_4:Eu^{3+}$ scintillator as detector for fiber optic dosimetry, Radiat. Meas. 106 (2017) 650–656, https://doi.org/10.1016/j.radmeas.2017.03.015.
[17] M. Alharbi, S. Gillespie, P. Woulfe, P. Mccavana, S. O'Keeffe, M. Foley, Dosimetric characterization of an inorganic optical fiber sensor for external beam radiation therapy, IEEE Sens. J. 19 (2019) 2140–2147, https://doi.org/10.1109/JSEN.2018.2885409.
[18] M. Alharbi, M. Martyn, S. O'Keeffe, F. Therriault-Proulx, L. Beaulieu, M. Foley, Benchmarking a novel inorganic scintillation detector for applications in radiation therapy, Phys. Med. 68 (2019) 124–131, https://doi.org/10.1016/j.ejmp.2019.11.018.
[19] Y. Shao, S.R. Cherry, S. Siegel, R.W. Silverman, S. Majewski, Evaluation of multi-channel PMTs for readout of scintillator arrays, Nucl. Instrum. Methods Phys. Res. A 390 (1997) 209–218, https://doi.org/10.1016/S0168-9002(97)00379-3.
[20] T. Yanagida, K. Kamada, N. Kawaguchi, Y. Fujimoto, K. Fukuda, Y. Yokota, V. Chani, A. Yoshikawa, Basic study of single crystal fibers of Pr:$Lu_3Al_5O_{12}$ scintillator for gamma-ray imaging applications, Nucl. Instrum. Methods Phys. Res. A 652 (2011) 256–259, https://doi.org/10.1016/j.nima.2010.08.114.
[21] M. Kim, W. Yoo, B. Lee, Development of a fiber-optic gamma endoscope to measure both optical and gamma images in a confined space, Opt. Express 25 (2017) 20087–20097, https://doi.org/10.1364/OE.25.020087.
[22] J. Zubia, J. Arrue, Plastic optical fibers: an introduction to their technological processes and applications, Opt. Fiber Technol. 7 (2001) 101–140, https://doi.org/10.1006/ofte.2000.0355.
[23] Y. Koike, K. Koike, Progress in low-loss and high-bandwidth plastic optical fibers, J. Polym. Sci. B 49 (2011) 2–17, https://doi.org/10.1002/polb.22170.
[24] J. Zhang, Y. Xiang, C. Wang, Y. Chen, S.C. Tjin, L. Wei, Recent advances in optical fiber enabled radiation sensors, Sensors 22 (2022) 1126–1148, https://doi.org/10.3390/s22031126.
[25] Z. Lin, S. Lv, Z. Yang, J. Qiu, S. Zhou, Structured scintillators for efficient radiation detection, Adv. Sci. 9 (2022), 2102439–2102464, https://doi.org/10.1002/advs.202102439.
[26] Epic Crystal, GAGG(Ce) scintillator datasheet. https://www.epic-crystal.com/oxide-scintillators/gagg-ce-scintillator.html.
[27] Mitsubishi Chemical, ESKA PREMIER Technical Sheet 1, https://pofeska.com/pofeskae/download/02.html.
[28] Hamamatsu, Photon counting head H11890 series datasheet. https://www.hamamatsu.com/jp/en/product/optical-sensors/pmt/pmt-module/photon-counting-head/H11890-210.html.
[29] R.W. Schafer, What is a Savitzky-Golay filter? IEEE Signal. Process. Mag. 28 (2011) 111–117, https://doi.org/10.1109/MSP.2011.941097.
[30] J.-H. Kim, G.-W. Jeung, J.-W. Lee, K.-S. Kim, Performance evaluation of a two-dimensional Savitzky-Golay filter for image smoothing applications, in: A. Hussain (Ed.), Electronics, Communications and Networks V, Lecture Notes in Electrical Engineering, vol. 382, Springer, Singapore, 2016, pp. 309–316, https://doi.org/10.1007/978-981-10-0740-8_35.